Bohnhoff, M., Zoback, M. D., Chiaramonte, L., Gerst, J. L., Gupta, N. (2010): Seismic detection of CO2 leakage along monitoring wellbores. - International Journal of Greenhouse Gas Control, 4, 4, 687-697

DOI: 10.1016/j.ijggc.2010.01.009

Seismic Detection of CO_2 Leakage along Monitoring Wellbores

Bohnhoff, M.[1,2] , Zoback, M.D.[1] , Chiaramonte, L.[1, *] , Gerst, J.L.[3] , Gupta, N.[3]

[1] Department of Geophysics, Stanford University, [2] Helmholtz-Centre Potsdam-GFZ, Germany, [3] Battelle Memorial Institute, Columbus, Ohio. * Now at Lawrence Livermore National Laboratory.

Abstract

A pilot carbon dioxide (CO_2) sequestration experiment was carried out in the Michigan Basin in which ~10,000 tonnes of supercritical CO_2 was injected into the Bass Island Dolomite (BILD) at 1050 m depth. A Passive Seismic Monitoring (PSM) network was operated before, during and after the ~17 day injection period. The seismic monitoring network consisted of two arrays of eight, three-component sensors, deployed in two monitoring wells at only a few hundred meters from the injection point. 225 microseismic events were detected by the arrays. Of these, only one event was clearly an injection-induced microearthquake. It occurred during injection, approximately 100 m above the BILD formation. No events, down to the magnitude -3 detection limit, occurred within the BILD formation during the injection. The observed seismic waveforms associated with the other 224 events were quite unusual in that they appear to contain dominantly compressional (P) but no (or extremely weak) shear (S) waves, indicating that they are not associated with shear slip on faults. The microseismic events were unusual in two other ways. First, almost all of the events occurred prior to the start of injection into the BILD formation. Second, hypocenters of the 94 locatable events cluster around the wells where the sensor arrays were deployed, not the injection well. While the temporal evolution of these events show no

correlation with the BILD injection, they do correlate with CO_2 injection for enhanced oil recovery (EOR) into the 1670 m deep Coral Reef formation that had been going on for ~2.5 years prior to the pilot injection experiment into the BILD formation. We conclude that the unusual microseismic events reflect degassing processes associated with leakage up and around the monitoring wells from the EOR-related CO_2 injection into the Coral Reef formation, ~700 m below the depth of the monitoring arrays. This conclusion is also supported by the observation that as soon as injection into the Coral Reef formation resumed at the conclusion of the BILD demonstration experiment, seismic events (essentially identical to the events associated with the Coral Reef injection prior to the BILD experiment) again started to occur close to a monitoring arrays. Taken together, these observations point to vertical migration around the casings of the monitoring wellbores. Detection of these unusual microseismic events was somewhat fortuitous in that the arrays were deployed at the depth where the CO_2 undergoes a strong volume increase during transition from a supercritical state to a gas. Given the large number of pre-existing wellbores that exist in depleted oil and gas reservoirs that might be considered for CO_2 sequestration projects, passive seismic monitoring systems could be deployed at appropriate depths to systematically detect and monitor leakage along them.

Keywords: CO_2 geological storage, Passive Seismic Monitoring, Induced seismicity, CO_2 leakage

Introduction

A pilot carbon dioxide (CO_2) sequestration project was carried out in Otsego County in the northern part of the Michigan Basin (Figure 1a). This project is part of the Midwest Region Carbon Sequestration Partnership (MRCSP, www.mrcsp.org), funded by the Department of Energy/National Energy Technology (DOE/NETL) and several co-sponsors. Potential target formations for sequestration in the frame of MRCSP projects include Paleozoic reservoirs, and in particular, Upper Silurian to Middle Devonian strata. The objectives of the demonstration project at this site were to evaluate the injectivity, storage capacity and overall suitability of the Bass Island Dolomite (BILD), a saline aquifer at 1050 m depth as a potential repository for CO_2 separated from natural gas produced from the Antrim shale (see Figure 1b for a generalized stratigraphic column in the target area obtained from borehole logs and cores). As will be shown, this demonstration experiment also provided the opportunity to detect and monitor potential leakage of CO_2 up pre-existing wellbores near the injection well. Given the very large number of pre-existing wells in depleted oil and gas reservoirs that might be considered for long term storage of CO_2, it is important to have a suite of monitoring strategies in place to assure that migration is not occurring through the caprock, along pre-existing sub-vertical faults or fracture zones or along pre-existing oil and gas production wells that may have been improperly plugged or whose cements may have been incomplete or corroded (e.g. Celia et al., 2004; Duguid et al., 2004).

During our pilot experiment a total of 10,241 metric tonnes of supercritical CO_2 were injected through a vertical well that was drilled in 2006 and that was perforated at the depth of the target formation. The CO_2 for this pilot injection project was separated from natural gas produced from the Antrim Shale at six centralized gas-processing plants in Otsego and adjacent counties. These plants produce ~1.2 million metric tons of CO_2 per year. The CO_2 is delivered to the test site through a pipeline that has been utilized for CO_2-EOR projects into the Coral Reef reservoir at approximately 1670 meters depth in the area.

The test interval for the demonstration project comprises the Bass Island Dolomite (BILD) and the Bois Blanc formations at ~1050 m. The BILD formation is a porous dolostone at the top of the Silurian Bass Islands group which is found throughout the Michigan Basin at an average thickness of 15 m (Figure 1). Its local thickness is 22 m and no major structural complexities are reported. Analysis of core samples for the formation indicated an average porosity of 13% and an average permeability of 22 mD. However, analysis of pressure response during and after CO_2 injection as well as the calibration of the model simulations indicates that the actual permeability is more than 50 mD (Sminchak et al., 2009). Barnes et al. (2008) present a geologic interpretation based on cores from the BILD injection well. The authors suggest that the target unit was deposited in a restricted marine, possibly tidal flat, environment with periodic and possibly protracted, subaerial exposure surfaces that resulted in repeated karsted intervals. They indicated that mineralized natural fractures are common. The Bois Blanc Formation is overlying the BILD formation and described as a cherty carbonate strata of 78 m thickness (Figure 1b). Although it could locally be considered as a seal due to the apparent lack of suitable injectivity potential, it has been mentioned in other parts of the Michigan basin as another potential storage target. At the injection site, the BILD formation is considered as primary storage interval. The primary caprock is the Amherstburg-Lucas Formation (see Figure 1b), a dense limestone with very low porosity and permeability. Like the BILD formation, it has a laterally uniform thickness of ~80 m. Porosity values are mostly less than 5%. Permeability measurements showed very low permeability, mostly less than 1 mD. The unit was described from cores as a fossiliferous, dense, skeletal wackestone to mud-rich packstone unit that shows good potential as an effective caprock (Barnes et al., 2008).

Figure 2 shows the geometry of the wells involved in the combined CO_2 injection and Passive Seismic Monitoring (PSM) campaign. Two seismic sub-arrays of eight three-component sensors each were deployed in two monitoring wells at 150 and 550 m lateral distance to the BILD injector, respectively (see also Figure 3). The aperture of each array is 105 m and the sensors (indicated by the triangles) have a 15 m equidistant spacing. The

eastern monitoring well is vertical. The western monitoring well consists of an older abandoned vertical section and a recently completed deviated (11° to the WNW) section that extends down to 1200 m, i.e. through BILD but not into the Coral Reef. The original vertical section of this well below 530 m was plugged and abandoned. Both monitoring wells were originally drilled in the 1970s and extend down to the Coral Reef. The surface position of the Coral Reef injection well is located close to the western monitoring well and deviated towards the north.

Figure 4 summarizes the injection flow rates into the BILD formation and the associated downhole pressure within BILD. It also shows the daily rate of the detected microseismic activity and the fluid flow rates into the Coral Reef for the same time period. The BILD injection started on Feb 8, 2008 (Julian day 39), injecting at ~7 million cubic feet per day (mmcf/d) for about two days. During that time no remarkable increase of the downhole pressure at the injection well was observed. After a five-day shut-in phase (days 41-46) a second test injection into BILD at a maximum flow rate of up to 20 mmcf/d (20 million cubic feet/day) was performed on day 46. Note, that the EOR-related injection into the Coral Reef had to be interrupted during BILD injections as the same infrastructure at the surface (pipelines) was used for either injection. Interestingly, both short-term BILD injections resulted in an almost instantaneous decrease in seismicity rate. The main injection into the BILD formation started on day 49 and resulted in a pressure maximum of 8.5 MPa. After a drop in pressure during continued injection throughout day 74 a slow but systematic increase in pressure is observed reaching a plateau at ~7.5 MPa. Upon completion of the BILD injection pressure slowly decreased. Analysis of the pressure response for the BILD injection test is presented in Sminchak et al. (2009).

Prior to the demonstration project in the BILD formation, injection into the deeper Coral Reef reservoir had gone on (at injection rates as high as 12 mmcf/day) for 2.5 years (non-continuously) and was stopped on day 39 after injecting at rates as high as 12 mmcf/d. After a one-day break (day 41) injection into the Coral Reef continued until day 50. Different than for the BILD injection only 1 day averages of the Coral Reef injection rates are available.

After effective termination of the BILD injection on day 67 the Coral Reef injection was resumed. The temporal evolution of the microseismicity is discussed in detail in the following section.

Downhole Passive Seismic Monitoring (PSM) of the CO_2 injection

One principal monitoring objective of the Michigan Basin Injection Experiment was to evaluate whether the CO_2 injection into the BILD formation would be accompanied by induced microseismicity. At the same time, this experiment was seen as a generic study investigating the potential of PSM to monitor CO_2 storage in similar formations in the region. Pressure increases associated with CO_2 injection into deep formations will reduce effective normal stresses on pre-existing faults, potentially leading to induced microseismicity and permeability enhancement. PSM is a well-established technique and is frequently applied during hydraulic fracturing operations for permeability enhancement in the hydrocarbon and geothermal industries (e.g. Rutledge et al., 1994; Shapiro, 2008). PSM is also used to detect gas and/or fluid flow behind casing with acoustic sensors deployed in wellbores (e.g. Smolen, 1995). Elevated average *noise* amplitudes are indicative of behind-casing flow. Bakulin and Korneev (2008) demonstrate that behind-casing fluid flow can induce tube waves (see White, 1983) that are detectable with PSM instrumentation.

The great majority of induced microearthquakes triggered during reservoir stimulation are typically of extremely small magnitude and thus cannot be detected at hypocentral distances greater than a few hundred meters (e.g. at the surface). Changes in the number of microearthquakes can be correlated with changes in the fluid-injection rates and pressure perturbations. Microseismic activity usually starts close to the injection point where pressure increases are largest. The hypocentral cloud then migrates away from that initial location following preferred orientations predefined by the local stress-field orientation or local fault structure (see Shapiro, 2008 for examples). Because there is the need is for PSM with as low

a magnitude detection threshold as practical, PSM is usually carried out with seismometers in monitoring wells within several hundred meters of an injection well. Microseismic monitoring was selected for this project because there are two accessible wells for monitoring near the injector well (at only 150 and 550 m lateral distance, respectively; see Figures 2 and 3) and extending down to the BILD target formation. A downhole seismometer array consisting of eight, three-component sensors was deployed in each well. Both arrays have an overall aperture of 105 m with equidistant sensor spacing of 15 m (Figure 3). Array 1 was deployed in the vertical eastern monitoring well at 550 m lateral distance to the injection point. Array 2 was deployed in the recently recompleted western monitoring well. Both seismic arrays were deployed slightly above BILD at ~900-1000 m true vertical depth. This exceptionally good network geometry allowed to monitor potentially induced microseismic activity within the BILD formation down to magnitudes as low as -3.0 (Engineering Seismology Group, pers. comm.). The PSM field campaign and pre-processing of the seismic recordings was conducted by Engineering Seismology Group, Kingston/CA (www.esg.ca). A total of seven calibration shots were fired inside the BILD injector well on day 24, directly after the seismic arrays were deployed but several weeks before the BILD injection commenced. Shots were fired at two distinct depth levels in order to record incoming seismic waves at two different incidence angles. The recordings of the shots served to ensure the functionality of the seismic arrays and recording system, to determine the orientation of the sensors at depth from the polarization of the P-waves and to calibrate the velocity model. The signal-to-noise ratios obtained from the shots were adequate to allow us to reliably determine the azimuth and incidence angles of the incoming rays. A waveform example showing the vertical components of all 16 sensors of one of the calibration shots is shown in Figure 5a. All seven shots were located with a precision of ~20 m. Clear P and S phase onsets were identified for each of the shots on both arrays. Since S phases would not be generated by an explosive source in an isotropic environment, the observed S phases most probably represent ‘quasi-shear’ waves indicating the existence of anisotropy in the near-by rock formation (Ben-Menahem et al., 1991). To check the consistency of the picked

phases and determine the P- to S-wave velocity ratio (v_p/v_s) for the area between the wells we plotted Wadati diagrams (Wadati, 1933). Therein, the differential travel time between P and S wave (T_s-T_p) at either sensor is plotted against T_p. Assuming a constant v_p/v_s ratio for the various travel paths of the seismic waves, the data of all sensors should fall on a line. Thus, the quality of the line fit is a measure of the consistency of the data set. Figure 5b shows the Wadati diagram for the recordings of all seven shots demonstrating the high consistency of the data set. The obtained average v_p/v_s ratio is 1.84 for the volume sampled by the elastic waves which is in good agreement with a value of 1.90 obtained from sonic logs in the wells at the relevant depth interval.

Seismic monitoring was carried out between days 23 and 70 continuously recording at a 4 kHz sampling rate. During that time period a total of 817 “triggers” were observed on the seismic arrays. 770 of the events were detected only at array 1 in the eastern monitoring well while only 39 events were detected at array 2 in the western monitoring well. Only eight events were recorded at both arrays of which seven were the calibration shots. The difference in number of detections cannot be explained by a difference of the overall noise conditions in the two monitoring wells as indicated from analysis of background noise levels at each particular sensor. Some sensors (sensor 5 of array 1; sensor 16 of array 2) did show a substantial higher noise level than others and were excluded from any further data processing in the following.

Data processing and spatiotemporal occurrence of microseismicity

Each of the 817 detected events was inspected individually to separate ‘seismic events’ from ‘non-seismic’ detections such as spikes, electronic noise or non-seismic signals of unknown origin. Thereafter, a total of 225 events were classified as ‘microseismic events’ and considered for further evaluation. 201 out of the 225 microseismic events were detected only

at array 1 while 23 were detected only at array 2. Only a single microseismic event was seen on both sensor arrays. Interestingly, the vast majority of the 225 seismic events occurred during the first days of the monitoring period and the seismicity rate decays to almost zero before the shallow injection into the BILD formation was even started. This was completely unexpected as fluid-injection induced microseismicity is expected to start only after the onset of injection.

Onset times of the different seismic phases were picked manually in the seismograms. Several distinctly different frequency characteristics of the P waves were observed in the seismic recordings. Figure 6 gives an overview on the most common types of waveform characteristics. A large number of events contain prominent secondary phases that appear to be S phases. However, the v_p/v_s ratios calculated from the apparent S-P differential travel times would correspond to nonphysical values for Poisson's ratio for geologic formations. Nor do the apparent S-P times agree with the values determined from analysis of the calibration shots (1.84) and sonic logs (1.90). Most importantly, the inversion of the P and apparent S onset times did not converge towards reliable hypocenters. Determining the phase velocities across the sensor arrays of the first and secondary arrival times we obtained values of typically 4.8 ±0.2 km/s (P waves) and 1.5 +/- 0.1 km/s (secondary phases), respectively. While 4.8 km/s reflects the compressional wave velocity of the surrounding rock formation (P waves), the secondary phases are not S waves but appear to be tube waves. Tube waves are waves propagating along a well with the speed of the borehole fluid. Tube waves are a well-known phenomenon in borehole seismology (e.g. White, 1983; Paillin and Cheng, 1991) with early observations dating back to the 1950s (Summers and Broding, 1952; Vogel, 1952). Tube waves are generated in a variety of ways, one of which is when an incoming elastic wave passes a discontinuity (i.e. a density contrast). The density contrast may be represented by the well itself, a strong impedance contrast in the formation surrounding the well, a change in casing size or a body inside the well. Once generated, tube waves propagate in both directions along the well with little energy loss. This is exactly what we observe along both of the two seismic arrays. In our case, either the monitoring wells or the

geophone arrays themselves probably represent the requisite density contrast (fluid versus rock formation, steel versus fluid) inside the well needed to generate tube waves. These tube waves then propagate to either side along the arrays and, in some cases, are even back-reflected at the end of the array (Figure 6a).

Almost all of the 225 events identified as induced seismic signals, therefore, do not appear to represent shear failure on reactivated fault patches due to increased fluid pressure as one would expect in fluid injection experiments. This is especially important with respect to the unusual location of the hypocenters as discussed below. Only one event (on day 56) had typical P and S phases and appears to be an expected injection-induced microseismic event associated with shear slip on a pre-existing fault or fracture. The waveforms recorded by the vertical components of all 16 sensors are shown in Figure 6g. Using the hypocentral location techniques described below, this event was found to be located between the two sensor arrays (it was the only event, other than the calibration shots, detected on both arrays). It was also the only locatable event that occurred during the injection into the BILD formation. As shown in Figure 3, this event is located ~100m above and some ~250 m to the southeast of the injection point (see also Figure 4 where this event is indicated as ‘shear event’).

A number of sensors exhibited a ringing signal after the P onsets. Such a signal may either be caused by a reverberating casing that is not properly bonded to the formation by cement, or by bad coupling of the sensor to the casing. Regardless of the exact origin of these reverberations, we performed a frequency analysis for each of the events at each sensor to exclude the ringing signals by digital filtering of the affected traces. We removed 60 Hz noise in the same manner. The striking observation from the frequency analysis was that most events exhibit distinct dominant frequencies (see Bohnhoff and Zoback, subm., for details). After noise removal, we classified the events into categories based on their different frequency characteristics (Table 1): A-type events have dominantly higher frequency contents, typically between 300 and 1000 Hz (~300-500 Hz is most pronounced) (Figure 6a+b). In contrast, B-type events have dominantly lower frequency contents, typically

between 40 and 150 Hz (~100 Hz is most pronounced) (Figure 6d+e). Note, that a substantial number of A- and B-type events have smaller portions of lower and higher frequency signals, respectively. B-type events on average have larger amplitudes and are partly even clipped on the sensors nearest to the source. As a third category, C-type events have clear contents of both frequency ranges with varying portions (Figure 6c+f). Some of the type A-C events have clear precursor signals (Figure 6c). A number of extremely weak events were detected (usually on only 4-5 sensors) but were so small as to prevent further analysis. As described in more detail by Bohnhoff and Zoback (subm.) event types A-C are interpreted to represent similar seismic source processes.

Hypocenters were determined by applying a least-square inversion to the P wave arrival times at the individual sensors of the arrays. A homogeneous velocity model with v_p=4.8 km/s was used and the position of the sensor with the earliest arrival time served as the starting location for the inversion. As we are inverting only P wave arrival times (but no shear-wave arrival times) we do not have information on sensor-specific source distances. Particle motion analysis for the individual three-component recordings did not result in stable azimuth determinations for the events. Therefore, the actual inversion is performed in 2D and the obtained hypocenters contain information about depth and lateral distance to the array, but there is no information about the azimuthal position. As a consequence, we project the hypocenter locations onto an EW-trending depth section in Figure 3 for illustration purposes only. We obtained a total of 94 stable hypocenter locations. All of the events were found to be located in the direct vicinity of one of the arrays (80 and 13 events at the eastern and western array, respectively) with a maximum lateral distance from the relevant array of 35 meters (Figure 3). The majority of events occurred near the shallower portion of the arrays. In addition, a total of 40 events produced clear P onsets on the sensors but occurred above or below the arrays (e.g. Figure 6 a+b), not permitting us to determine their exact source location. However, the rapid decay of P wave amplitudes across the array indicates that these events have occurred in very close vicinity to the arrays since typically 2-3 sensors were located in the seismic near field (further discussed in Bohnhoff and Zoback, subm.).

These events are summarized and indicated by the open circles in Figure 3. With the average picking accuracy for the P onset times of 0.25 msec the precision of the hypocenters is in the range of 5 meters for the events near the arrays. No microseismic events down to magnitude -3 were found to have occurred at the depth of the BILD formation. The magnitude for the single shear event was found to be -2.3. Determation of magnitudes for the other events was not possible since typically 2-3 sensors were located in the seismic near field where the 3D-particle motion is highly non-linear (e.g. Vavrycuk, 1992; see Bohnhoff & Zoback, subm., for details). The remaining number of sensors then was not sufficient to reliably calculate magnitudes.

Discussion

It is widely recognized that events detected during PSM of fluid-injection operations result from slip on pre-existing faults, sometimes revealing a network of intersecting fractures (e.g. Rutledge et al., 1994; Baisch and Harjes, 2003; Shapiro, 2008; Lei et al., 2008). Even during hydraulic fracturing operations, the hydrofrac acts as a source of fluid pressure that stimulates slip on the pre-existing fracture and fault network, but is not itself the origin of the great majority of the seismic events. Hypocenters typically cluster into well-defined small-scale geometrical patterns (e.g. Philips et al., 2002) and the enhanced use of such data sets has made significant progress in recent years applying location collapsing methods (Jones and Stewart, 1997) as well as relative relocation techniques (Waldhauser and Ellsworth, 2000).

In the case of the CO_2 injection into the BILD formation, we did not expect to create a hydraulic fracture because the injection pressure did not exceed the least principal stress at depth. Instead, we expected to determine if shear slip on pre-existing faults and fractures within the storage formation was induced by the increased pore-fluid pressure. Prior to the BILD injection, a packer was installed in the western monitoring well below the sensor array to prevent potential upward flow of CO_2 from the BILD formation inside the well. No such

packer was needed in the eastern monitoring well, because it was not perforated in the BILD formation.

As mentioned above, the majority of observed microseismic events occurred before the injection into the BILD formation even started (Figure 4). Hence, the observed microseismic events cannot be related to the BILD injection, both in terms of its spatial and temporal distribution. In contrast, the temporal occurrence of the induced microseismicity has a clear correlation with the EOR-related injection of supercritical CO_2 into the Coral Reef at 1670 m depth (Figure 4). As described above, the deeper injection was going on for about 2.5 years and was interrupted to carry out the BILD injection. It is likely, therefore, that the observed microseismicity reflects leaking CO_2 that potentially rises from the Coral Reef either along vertical interfaces (rock formation to cement and/or cement to casing), along gaps in the cement annulus of the monitoring wells, or along pre-existing fractures and cracks in direct vicinity around the monitoring wellbores during injection into the Coral Reef. Several other observations in Figure 4 further support this argument. First, the microseismic events stop when the deep injection stops after day 50. Second, microseismic events with the same characteristics as during the early phases of deep injection again occur on day 69 when the deep injection resumes (the sensor arrays stopped recording and were recovered on day 70).

The highest microseismicity rates are observed when flow rates of the deep injection reached maximum values of ~11 mmcf/d on day 38 (Figure 4) then declined after the Coral Reef injection was stopped to carry out the test injection into BILD. The microseismic activity again appeared during the Reef injection on days 42-50. The second test-injection into BILD lasted only a couple of hours and is not seen in the diagram of flow rates into the Coral Reef due to the daily sampling of the flow rate data. However, it is seen in the reduced seismicity rate. Once the major BILD injection commenced, seismicity then decreased to zero (except for the shear event and one unlocatable event) during the entire major phase of the BILD injection (day 50-67).

The single shear microseismic event that was detected above the BILD injection depth, and the complete absence of microseismic events in the BILD formation, raise a number of interesting questions. For example, because the shear event likely occurred along a pre-existing fault or fracture connected to the BILD formation, it is interesting that only one such event occurred as the likely pressure perturbation ~250m from the injection point (Fig. 3b) is likely extremely small. The absence of microseismic events within the BILD indicates that the pressure change within the formation during injection was inadequate to initiate slip on pre-existing faults. It cannot be ruled out that pressure changes in the BILD due to leakage from the Coral Reef over the past ~2.5 years caused slip on faults and/or fractures to occur in the past and effectively de-stressed the BILD formation.

The CO_2 is injected under high pressure as a supercritical fluid resulting in a complex multiphase fluid system within the Coral Reef reservoir. Fluid properties such as density, enthalpy and viscosity are essential for describing non-isothermal flow in porous media and depend on the pressure and temperature conditions and the exact fluid composition. Buoyancy due to gravitational forces plays an important role when CO_2 is injected into the subsurface because of its low density with respect to formation brines and water. Up flow of leaking CO_2 from the deep reservoir towards the surface would result in decreasing pressure and temperature eventually resulting in the CO_2 changing from a supercritical fluid to a gaseous phase. This process is accompanied by substantial volume expansion and reduction in average density.

The downhole pressure at the Michigan test site at the depth of BILD is essentially hydrostatic. Temperature measurements from more than 100 sites throughout the Michigan Basin indicate an average thermal gradient of 2.9 °C / 100 m (Gardner and Bray, 1984). Using the downhole pressure and thermal gradients as boundary conditions we calculated the density versus depth relation for pure CO_2 according to the Peng-Robinson Equation of State (PREOS) (A. Kovscek, pers. comm.). For the conditions relevant to this site, Fig. 7a indicates a systematic decrease of CO_2 density with decreasing depth. Moreover, the density gradient with depth has a pronounced maximum around 900 m (Figure 7a). This is exactly

the depth interval covered by the seismic arrays and microseismic events discussed above. The majority of events occurs towards the shallower part of the sensor arrays at ~930 m (see Figure 3), i.e. close to the maximum of the density gradient. We conclude that the observed microseismic events are triggered by the volume increase of the CO_2 during transition from supercritical to gaseous while leaking up along and/or around the annulus of the two monitoring wells. This helps explain the unusual characteristics of the seismic waveforms acquired by the two downhole seismic arrays (see Bohnhoff and Zoback, submitted). The density gradient reaches a maximum at ~900 m but Figure 7a suggests that degassing of CO_2 should also occur slightly above and below the arrays, perhaps at a lower activity level. This suggests that a small number of microseismic events may have occurred above and below the arrays but at such small magnitudes (presumably below M -3) they remained largely undetected.

The actual physical mechanism responsible for the leakage is not fully understood and requires further investigation. For simplification, we assume that a multi-phase system of CO_2, formation water and oil exists in the Coral Reef formation. Assuming that these phases do not interact over the time scale of injection due to buoyancy effects, the CO_2 will likely accumulate at the reservoir/cap rock interface. There, the significantly lower permeability of the cap rock would be expected to prevent the CO_2 from rising and acts as a seal unless a through-going permeable fault or a leaky wellbore were present. As described above, the Coral Reef injection has a nearly instantaneous impact on the seismicity rate, e.g. on day 69 induced microseismicity starts close to the eastern monitoring well right after injection into the Coral Reef was resumed. Since the migration velocity of injected CO_2 in the formation is expected to be relatively slow we conclude that the CO_2-degassing around the monitoring wellbores is caused by the injection into the Coral Reef and migration up along the monitoring wells.

A confirmation of the potential migration of CO_2 from the Coral Reef along wellbores and an assessment of physical mechanisms for the migration can only be made through additional characterization of wellbore and cement integrity in the Coral Reef wells. During

the experiment no CO_2 has been observed within the two monitoring wells. This, however, has no implication on the proposed leakage pathways outside the wells since the observed microseismic events clearly occurred behind the well casings and within the annulus or/and the nearby rock formation. The observed difference in seismicity rate along the two monitoring wells might be explained by the fact the eastern monitoring well (90% of the seismic events) directly penetrates into the Coral Reef while the sensors in the western monitoring well were deployed in the re-drilled deviated part that does not directly penetrates into the Coral Reef (Fig. 2). There, the main migration path for CO_2 might be the older abandoned vertical section from which a weak connection to the deviated section with the sensors might cause the substantially lower level of degassing events (see Figure 7b).

Conclusions

As illustrated in Figure 7b, it seems clear that the unusual (i.e., non-shear) microseismic events detected near the two monitoring arrays is due to the EOR-related injection into the Coral Reef formation and potential leakage of CO_2 along or around the well casings. The immediate occurrence of microseismicity ~700 m above the depth of injection following the resumption of the Coral Reef injection further demonstrates vertical hydraulic communication between the two depths probably due to leakage along and/or around the well casings. As the onset of seismicity occurs almost instantaneously after resuming injection into the Coral Reef it would appear the leakage is responding to the injection-related pressure in the Coral Reef rather than the CO_2 itself as its migration within the reservoir would be expected to take time to reach the position of the monitoring wells. To address remaining uncertainties regarding the evaluation of the exact migration pathways of the CO_2 further specifically designed monitoring is needed.

The fact that 90% of the detected events were observed at the eastern monitoring well and only few events were detected at the western monitoring well might result from the well trajectories and location of sensors. However, it might as well reflect the relative amount of leakage along the two wells, and therefore requires further investigation. As both seismic arrays had essentially equal noise levels, it does not appear to be a detection phenomenon.

The single shear microseismic event that was detected above the BILD injection point and the complete absence of microseismic events in the BILD formation raise a number of interesting questions. The shear event likely occurred along a pre-existing fault or fracture connected to the BILD formation. As the location of this event was ~250 m from the injection point, an extremely small pressure perturbation likely triggered the event. While the absence of microseismic events within the BILD indicates that the pressure change within the formation during injection was inadequate to initiate slip on pre-existing faults, it cannot be ruled out that pressure changes in the BILD due to leakage from the Coral Reef over the past ~2.5 years may have caused slip on faults and effectively de-stressed the BILD formation.

It was fortuitous that the placement of the seismic arrays was exactly at the depth where the density of the supercritical CO_2 changes abruptly in conjunction with volume increase as it changes to a gas. This said one could use knowledge of pressure and temperature at depth to systematically deploy seismic arrays at the depth where the CO_2 degassing is expected in order to use passive microseismic monitoring to detect and monitor leakage along pre-existing wellbores in. This is of relevance given more than a million pre-existing production wells in areas considered for CO_2 sequestration alone in North America.

Acknowledgements

We thank Engineering Seismology Group, Kingston/CA, for conducting the seismic field campaign and useful discussions. We also thank Norm Sleep, Bill Ellsworth and Jerry Harris

for fruitful discussions. We are grateful to the Deutsche Forschungs Gemeinschaft (DFG) for funding within the Heisenberg programme.

References

Baisch, S., Harjes, H.P., 2003. A model for fluid-injection-induced seismicity at the KTB, Germany. Geophys. J. Int., 152, 160-170.

Bakulin, A., Korneev, V., 2008. Acoustic signatures of cross flow behind casing in commingled reservoirs: A case study from Teapot Dome. Geophysics, 73(4), p.E145-E152.

Barnes, D.A., Harrison, W.B., Wahr, A., 2008. Assessment of regional geological carbon sequestration potential in Upper Silurian to Middle Devonian strata of the Michigan Basin. In: M. Grobe, J.C. Pashin, and R.L. Dodge, eds., Carbon dioxide sequestration in geological media – State of the science: AAPG Studies 59, p. 1-26.

Ben-Menahem, A., Gibson Jr, R.L., Sena, A.G., 1991. Green's tensor and radiation patterns of point sources in general anisotropic inhomogeneous elastic media, Geophys. J. Int., 107, 297-308.

Bohnhoff, M, Zoback, M.D., subm. to J. Geophys. Res. Oscillation of fluid-filled cracks triggered by degassing of CO_2 during leakage from its storage reservoir.

Celia, M., Bachu, S., Nordbotton, J.M., Gasda, S.E., Dahle, H.K., 2004. Quantitative Estimation of CO_2 Leakage from Geological Storage: Analytical Models, Numerical Models, and Data Needs. Paper 228, 7^{th} Int. Conf. on Greenhouse Gas Control Technologies, Vancouver, Canada, Sept 5-9.

Duguid, A., Radonjic, M., Bruant, R., Mandecki, T., Scherer, G., Celia, M., 2004. The effect of CO_2 Sequestration on Oil Well Cements, paper 123, 7^{th} Int. Conf. on Greenhouse Gas Control Technologies, Vancouver, Canada, Sept 5-9.

Gardner, W.C., Bray, E.E., 1984. Oils and Source Rocks of Niagaran Reefs (Silurian) in the Michigan Basin, in J.G. Palacas, ed., Petroleum geochemistry and source rock potential of carbonate rocks: AAPG Studies in Geology 18, p.33-44.

Jones, R.H., Stewart, R.C., 1997. A method for determining significant structures in a cloud of earthquakes. J. Geophys. Res., 102(B4), 8245-8254.

Lei, X., Yu, G., Ma, X., Wang, Q., 2008. Earthquakes induced by water injection at ~3 km depth within the Rongchang gas field, Chongqing, China. J. Geophys. Res., 113, B10310, doi:10.1029/2008JB005604.

Paillet, F.L., Cheng, C.H., 1991. Acoustic Waves in Boreholes, ISBN 0-8493-8890-2, CRC Press Inc., Boca Raton, Florida.

Phillips, W.S., Rutledge, J.T., House, L.S., Fehler, M.M.C., 2002. Induced Microearthquake Patterns in Hydrocarbon and Geothermal Reservoirs: Six Case Studies. PAGEOPH, 159, 345-369.

Rutledge, J.T., Phillips, W.S., Roff, A., Albright, J.N., Hamilton-Smith, T., Jones, S., Kimmich, K., 1994. Subsurface fracture mapping using microearthquakes detected during primary oil production, Clinton County, Kentucky, paper SPE 28384, Soc. of Petro. Eng. Ann. Tech. Conf.

Shapiro, S.A., 2008. Microseismicity: A tool for reservoir characterization. Education Tour Series CIS, EAGE, ISBN 978-90-73781-70-2, The Netherlands.

Sminchak, J., Gupta, N., Gerst, J., 2009. Well Test Results and Reservoir Performance for a Carbon Dioxide Injection Test in the Bass Islands Dolomite in the Michigan Basin. Envorinmental Geosciences, 16, 153-162.

Smolen, J.J., 1995. Cased hole and production log evaluation (chapter 14: Fluid Movement: Noise Logging). PennWell Books, ISBN 087814465X, 9780878144655, 365p.

Summers, G.C., Broding, R.A., 1952. Continuous velocity logging, Geophysics, 17, 598-614.

Vavrycuk, V. 1992. Polarization properties of near-field waves in homogeneous isotropic and anisotropic media: numerical modeling. Geophys. J. Int., 110, 180-190.

Vogel, C.B., 1952. A seismic velocity logging method, Geophysics, 17, 586-597.

Wadati, K., 1933. On the travel time of earthquake waves II, Geophys. Mag., 7, 101-111.

Waldhauser, F., Ellsworth, W.L., 2000. A Double-Difference Earthquake Location Algorithm: Method and Applications to the Northern Hayward Fault, California. Bull. Seismol. Soc. Am., doi:10.1785/0120000006.

White, J.E., 1983. Underground Sound: Application of Seismic Waves, Methods in Geochemistry and Geophysics, 18, Elsevier Amsterdam-Oxford-New York.

Table Captions:

Table 1:

Classification of seismic event types observed during passive seismic monitoring of CO_2 sequestration. Types were classified based on varying frequency contents of the events. See text for details.

Tables:

Table 1:

Event category	number of events	dominant frequency (range) [Hz]
A	15	~500 (300-1000)
B	33	~100 (40-150)
C	59	both dominant frequencies ranges of A and B type
shear event	1	
other	117	extremely weak, variable frequency

Figure captions:

Figure 1:

a) Depth of the Bass Island Dolomite (BILD) formation throughout the Michigan Basin. The red dot represents the location of the test site, where the combined CO_2 sequestration and downhole Passive Seismic Monitoring (PSM) experiment was carried out. The average thickness of the BILD layer throughout the Michigan Basin is 15 m and its local thickness at the injection site is 22 m. While regional changes of the depth of the BILD layer are considerable no major local variations in its depth (1050 m) are reported.

b) Stratigraphic column of the well used for CO_2 injection into the Bass Island Dolomite (BILD) at 1050 m depth and the overlying Bois Blanc Formation. The Amherstburg-Lucas formation was expected to act a seal against CO_2 leakage. LS= limestone. The Coral Reef was used for EOR-related CO_2 injection and is located at 1670 m depth. BILD and Coral Reef reservoirs are indicated by the black arrows.

Figures 2:

Geometry of the wells involved in the combined CO_2 injection and Passive Seismic Monitoring (PSM) campaign at the Michigan test site. Two seismic sub-arrays of eight three-component sensors each were deployed in two monitoring wells at 150 and 550 m lateral distance to the BILD injector, respectively. The aperture of either array is 105 m and the sensors (indicated by the triangles) have a 15 m equidistant spacing. The eastern monitoring well is vertical while the western monitoring well consists of an older abandoned vertical part and a new part that is deviated towards the WNW. The surface position of the Coral Reef injection well (dash-dotted) is located close to the western monitoring well and deviated towards the north. The open circles represent the surface location of either injection well whereas the stars represent the injection points at depth. Bars represent bridge plugs. The

geometry of the wells is shown in map view (a), and as depth section seen from the east (b) and the south (c). Target formations for the shallow (BILD) and deep (Coral Reef) injections are indicated by the bold lines.

Figure 3:

Blow-up of Figure 2 focusing on the downhole seismic network and the BILD injection well (the Coral Reef injection well is not shown). a) shows the map view and b) is a depth section seen from the south. Symbols are as in Figure 2. Dots represent hypocenters of the observed induced microseismicity. Open circles represent a total of 40 events that could not be located precisely but that are most likely located close to either end of one of the sub-arrays (see text for details). The only event seen on both sensor arrays was also the only shear event and is indicated in a) and b).

Figure 4:

Hydraulic and seismicity data from the Michigan Basin Injection Experiment. From top to bottom the diagrams show flow rates of the CO_2 injection into the BILD formation at 1050 m depth, downhole pressure in the BILD formation (measured in the BILD injection well), daily seismicity rate as detected by the downhole seismic network and flow rates of the EOR-related CO_2 injection into the Coral Reef reservoir at 1670 m depth. The time scale is uniform for all four diagrams in days of year in 2008. Notes that downhole pressure at BILD and flow into the Coral Reef are sampled 1/day only.

Figure 5:

a) Waveform example from a calibration shot conducted in the BILD injector at 977 m depth on the 24th January 2008, i.e. after deployment of the downhole seismic array and prior to the start of the BILD injection. Shown are the vertical components of the 16 sensors from both sensor sub-arrays (see Figure 3 for sensor location). Array 1: sensors 1-8, array 2: sensors

9-16. Clear P and (quasi)S phases are obtained at both sensor arrays. All seven calibration shots were fired in the BILD injection well.

b) Wadati diagram (Wadati, 1933) for the seven calibration shots. Plotted are the differential travel times between P and S wave (T_s-T_p) at each of the 16 sensors with T_p. Assuming a constant v_p/v_s ratio, the data of all sensors should fall on a line. Thus, the quality of the line fit is a measure of the consistency of the data set. The obtained average v_p/v_s ratio is 1.84 for the volume sampled by the elastic waves which is in good correlation with the results of 1.90 obtained from sonic logs along the wells at the relevant depth interval.

Figure 6:

Examples for the different waveform characteristics obtained from the induced microseismic events. For each event in subfigures a-f the vertical components of the eight sensors from the relevant seismic array are plotted (array 1: sensors 1-8, array 2: sensors 9-16; see Figure 3 for location of sensors). All seismograms are filtered with a Notch filter to eliminate 60Hz and multiples as well as individual ringing signals of the sensors. Picked phases are color-encoded (P wave=red, Tube wave=green, S wave=blue).

a) Type-A event with dominantly higher frequency contents of the P wave (~600-900 Hz) and clear tube waves that are generated at the upper end of the sensor array when the P wave enters the monitoring well (see text for details). The source is located slightly above the array. Later in the seismogram a tube wave reflected at the lower end of the sensor array is seen then propagating upwards.

b) Type-A event similar to the one in a) but with a hypocenter that is located within the depth extent of the array close to sensor 11.

c) Type-C event with dominantly higher (and some lower) frequency contents and a clear precursor phase at constant time offset prior to the P wave at all sensors. The precursor signal is interpreted to represent bubble-growth processes during the degassing of CO_2 from supercritical to gaseous (see Bohnhoff and Zoback, subm., for details).

d) Type-B event with dominantly lower (~80Hz) frequency contents. The event occurred close to sensor 3.

e) Type-B event with dominantly lower frequency contents of the P wave (~100Hz) although some higher frequencies can be seen on top of that. The P phase looks highly similar on all sensors with an upward pointing first motion polarity. The event is located close to sensor 4.

f) Type-C event with comparable contributions of lower and higher frequency contents on all sensors of the array. The event is located close to sensor 4.

g) Shear event: The only event with clear P and S phases indicating a shear source process. It was also the only event seen at both sensor arrays (see text for details).

Figure 7:

a) Depth versus density and density gradient for pure CO_2 calculated according to the Peng-Robinson Equation of State (PREOS) (Kovscek, pers. comm.). For the calculation we assumed hydrostatic pressure at the Michigan test site and a regional thermal gradient of 2.9 °C/100 m (Gardner and Bray, 1984). A systematically decreasing CO_2 density is observed with decreasing depth. The largest density gradient is observed at ~900 m depth, i.e. exactly where the sensor arrays were placed and where the density of the observed microseismic activity is highest. This supports the conclusion that the microseismic events are triggered by volume changes (degassing) of the CO_2 while rising towards the surface.

b) Schematic sketch for the observed CO_2 leakage from the Coral Reef reservoir to the depth interval of the seismic sensors where it expands from a supercritical state to gaseous (see text for details). Injection into the BILD and Coral Reef reservoirs is indicated by the white arrows, respectively. The exact pathways from the Coral Reef towards the location of the degassing signals around the sensor arrays remains unresolved but leakage along and/or around the wellbore annulus seems likely as cavities in the cement around the well casings would explain how rapidly events are observed at the monitoring arrays when the Coral Reef injection is resumed.

10. Figures:

a) b)

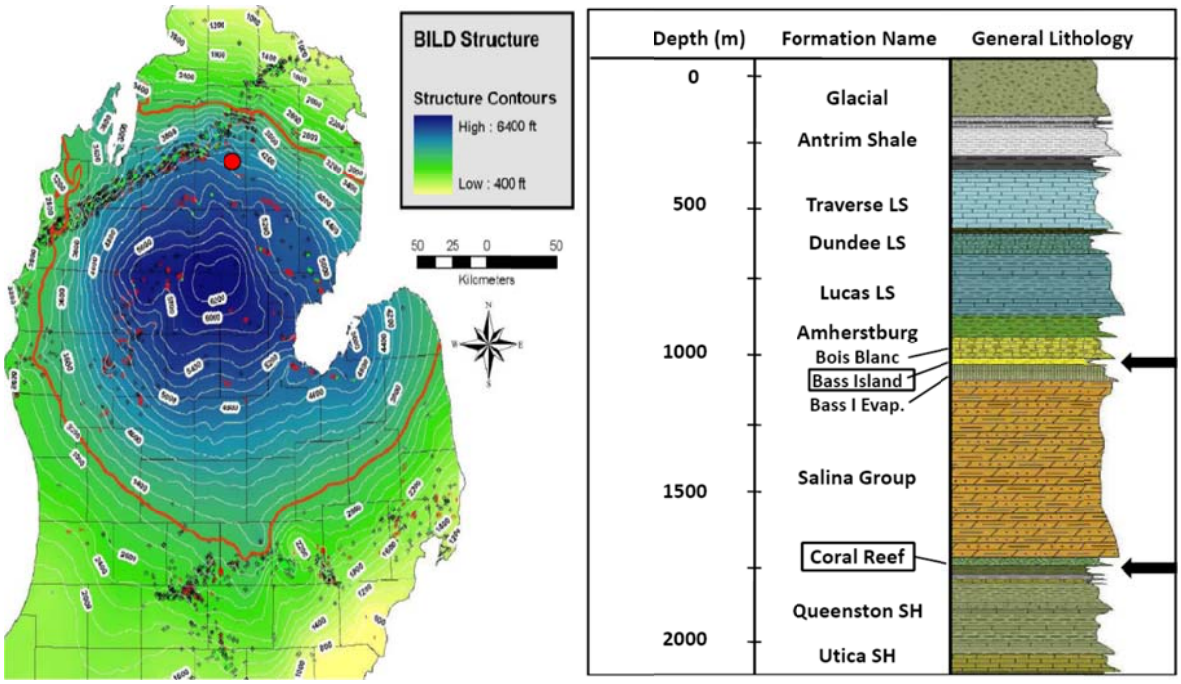

Figure 1

a)

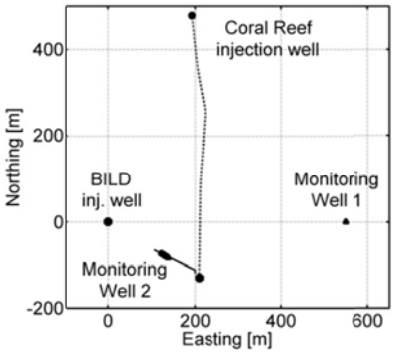
Coral Reef
injection well
BILD
inj. well
Monitoring
Well 1
Monitoring
Well 2
Northing [m]
Easting [m]
400
200
0
-200
0
200
400
600

b)

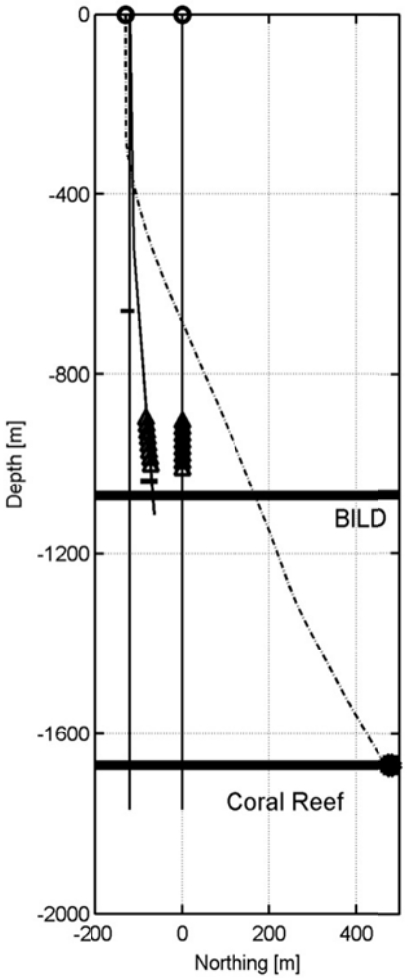
BILD
Coral Reef
Depth [m]
Northing [m]
0
-400
-800
-1200
-1600
-2000
-200
0
200
400

c)

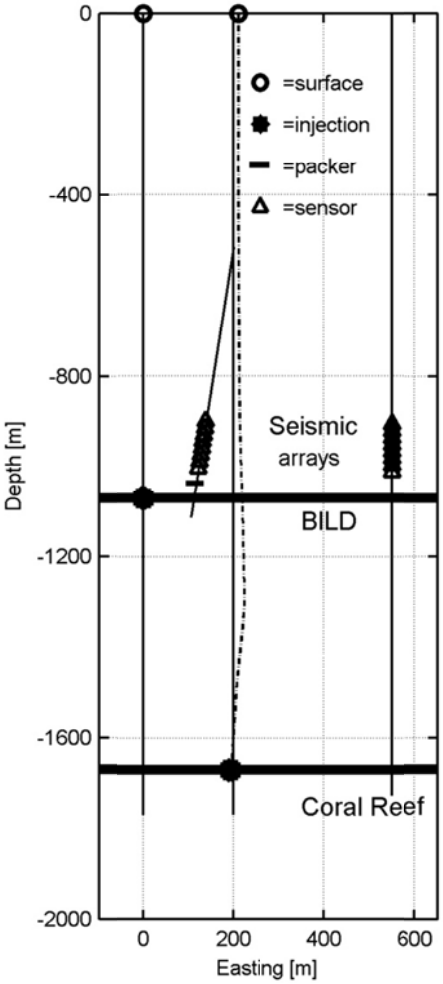
=surface
=injection
=packer
=sensor
Seismic
arrays
BILD
Coral Reef
Depth [m]
Easting [m]
0
-400
-800
-1200
-1600
-2000
0
200
400
600

Figure 2

a)

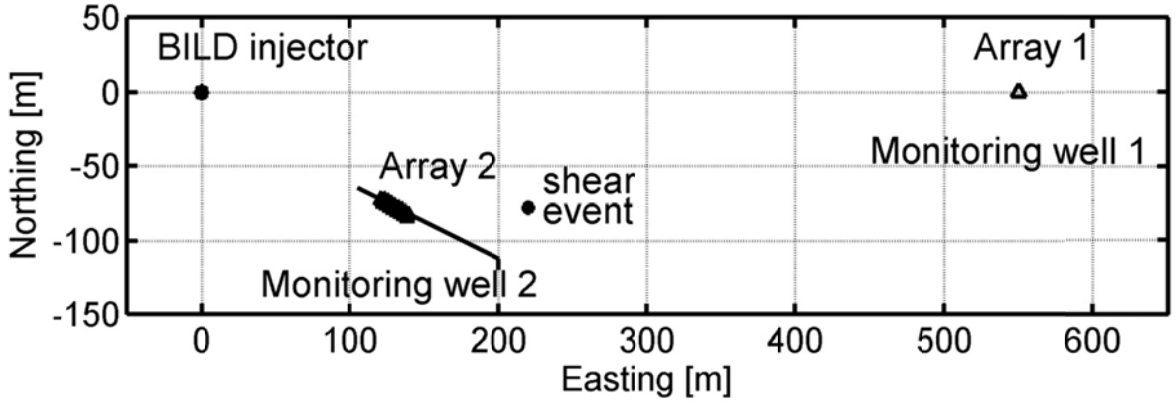
BILD injector
Array 1
Monitoring well 1
Array 2
shear
event
Monitoring well 2
Northing [m]
Easting [m]
50
0
-50
-100
-150
0
100
200
300
400
500
600

b)

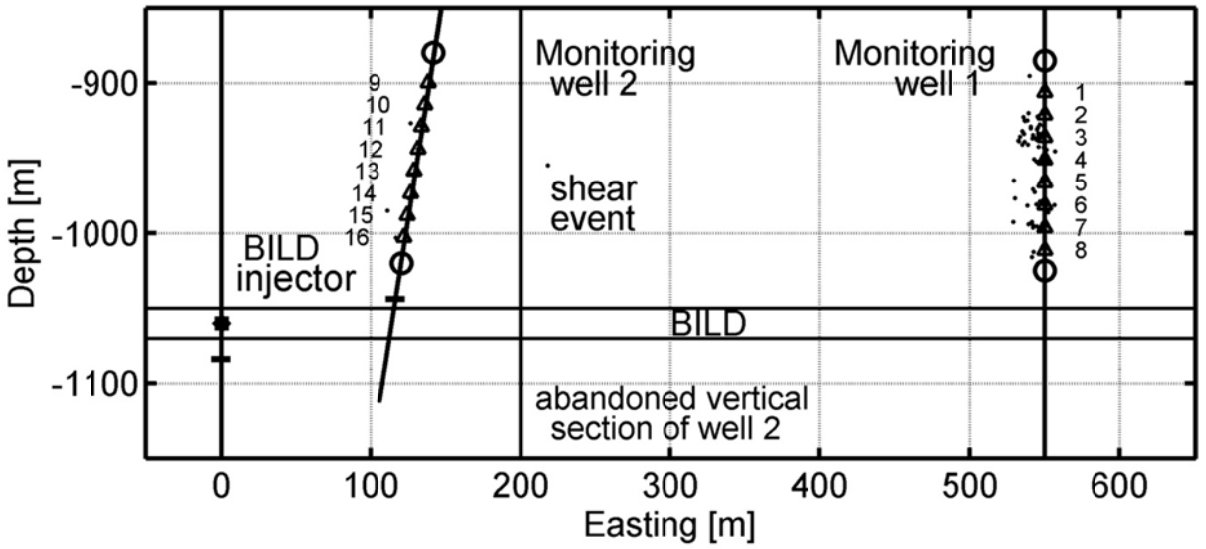
Monitoring
well 2
Monitoring
well 1
shear
event
BILD
injector
BILD
abandoned vertical
section of well 2
Depth [m]
Easting [m]
-900
-1000
-1100
0
100
200
300
400
500
600
9
10
11
12
13
14
15
16
1
2
3
4
5
6
7
8

Figure 3

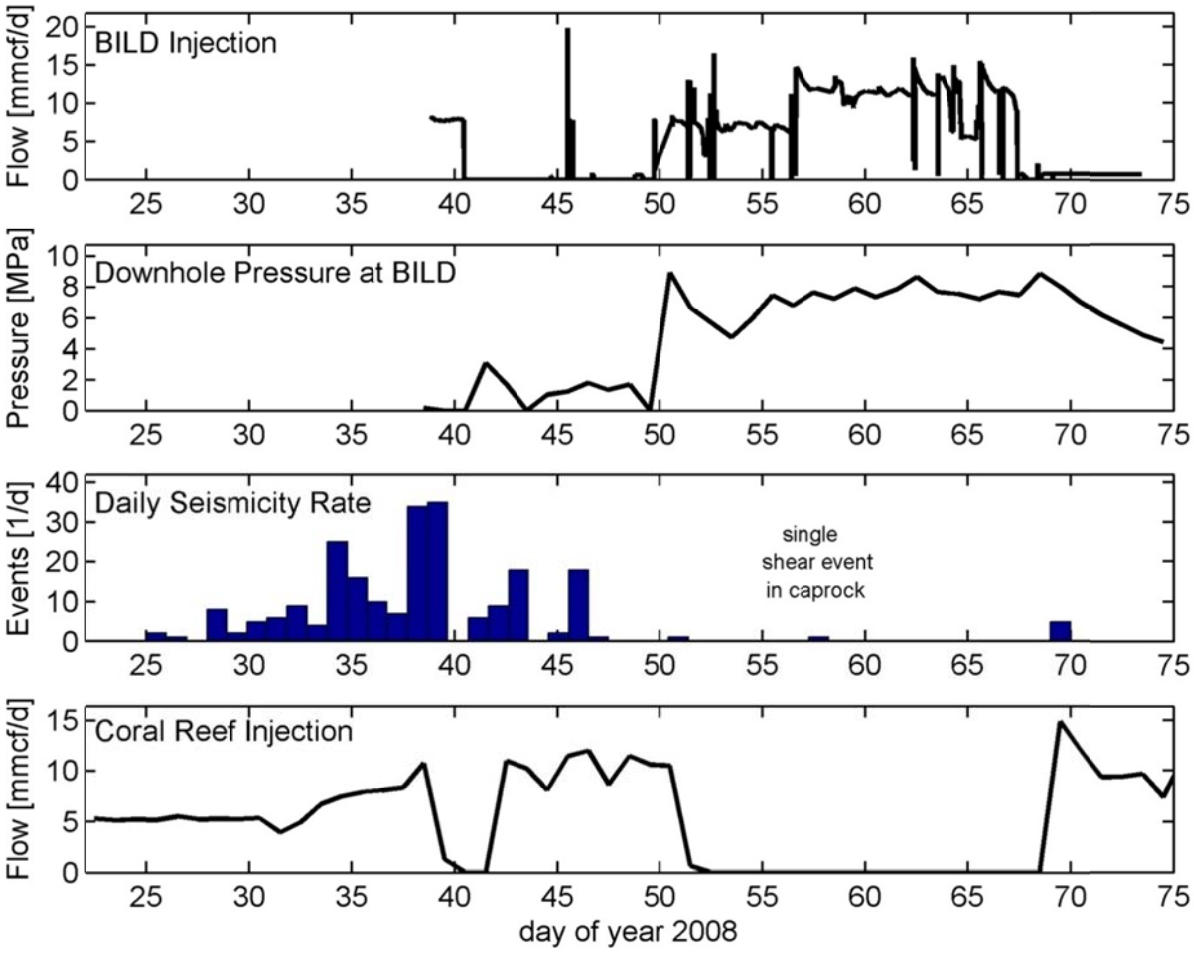
BILD Injection
Flow [mmcf/d]
Downhole Pressure at BILD
Pressure [MPa]
Daily Seismicity Rate
Events [1/d]
single
shear event
in caprock
Coral Reef Injection
Flow [mmcf/d]
day of year 2008

Figure 4

a)

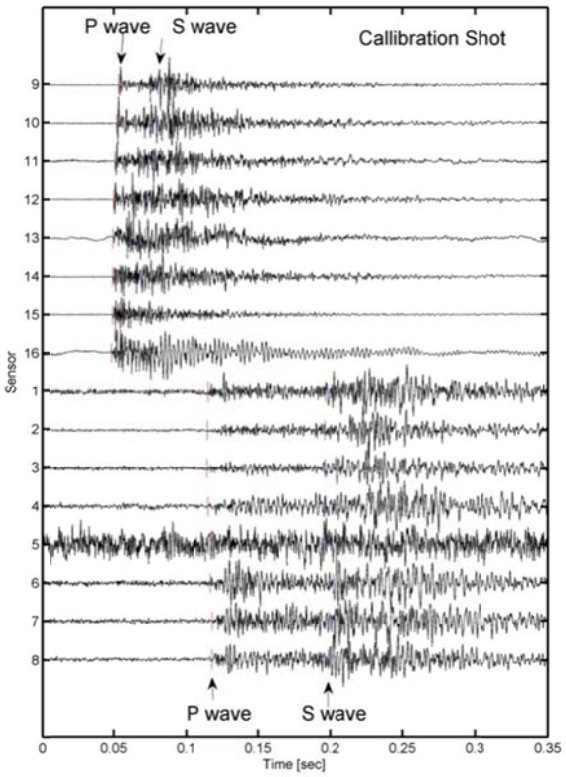
P wave
S wave
Callibration Shot
Sensor
9
10
11
12
13
14
15
16
1
2
3
4
5
6
7
8
P wave
S wave
0
0.05
0.1
0.15
0.2
0.25
0.3
0.35
Time [sec]

b)

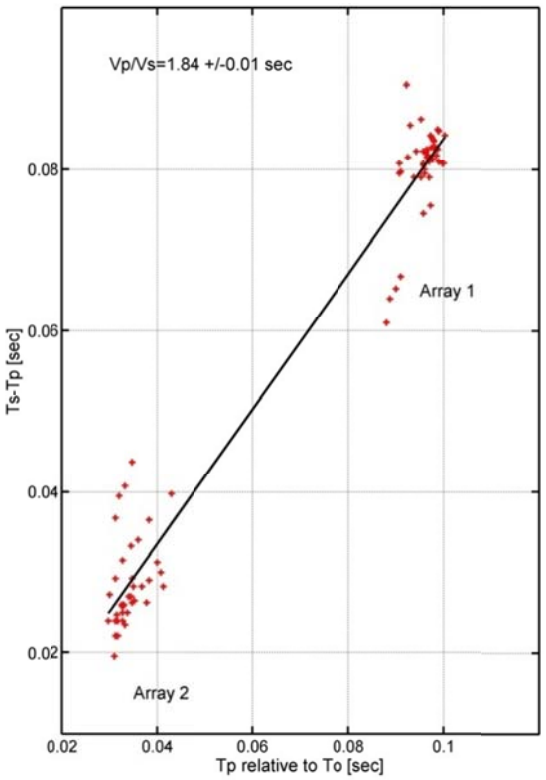
Vp/Vs=1.84 +/-0.01 sec
Array 1
Array 2
Ts-Tp [sec]
0.02
0.04
0.06
0.08
0.02
0.04
0.06
0.08
0.1
Tp relative to To [sec]

Figure 5

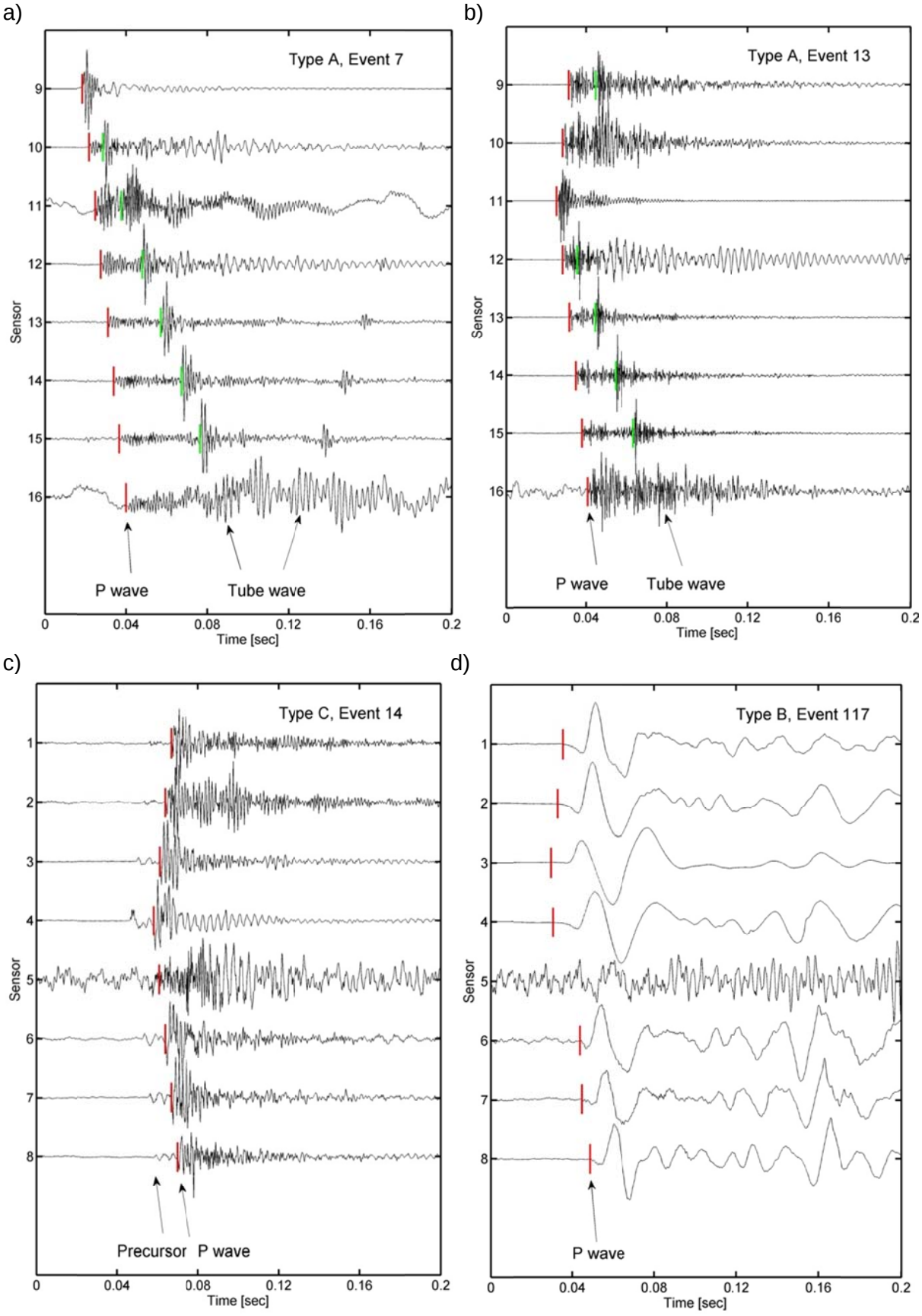
a)
Type A, Event 7
Sensor
9
10
11
12
13
14
15
16
P wave
Tube wave
0
0.04
0.08
0.12
0.16
0.2
Time [sec]
b)
Type A, Event 13
Sensor
9
10
11
12
13
14
15
16
P wave
Tube wave
0
0.04
0.08
0.12
0.16
0.2
Time [sec]
c)
Type C, Event 14
Sensor
1
2
3
4
5
6
7
8
Precursor
P wave
0
0.04
0.08
0.12
0.16
0.2
Time [sec]
d)
Type B, Event 117
Sensor
1
2
3
4
5
6
7
8
P wave
0
0.04
0.08
0.12
0.16
0.2
Time [sec]

Figure 6

e)

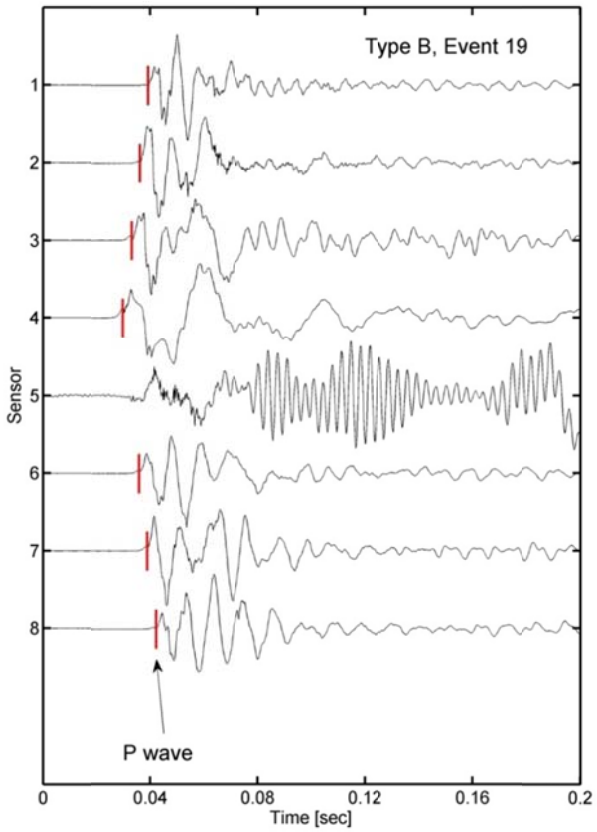
Type B, Event 19
Sensor
1
2
3
4
5
6
7
8
P wave
0
0.04
0.08
0.12
0.16
0.2
Time [sec]

f)

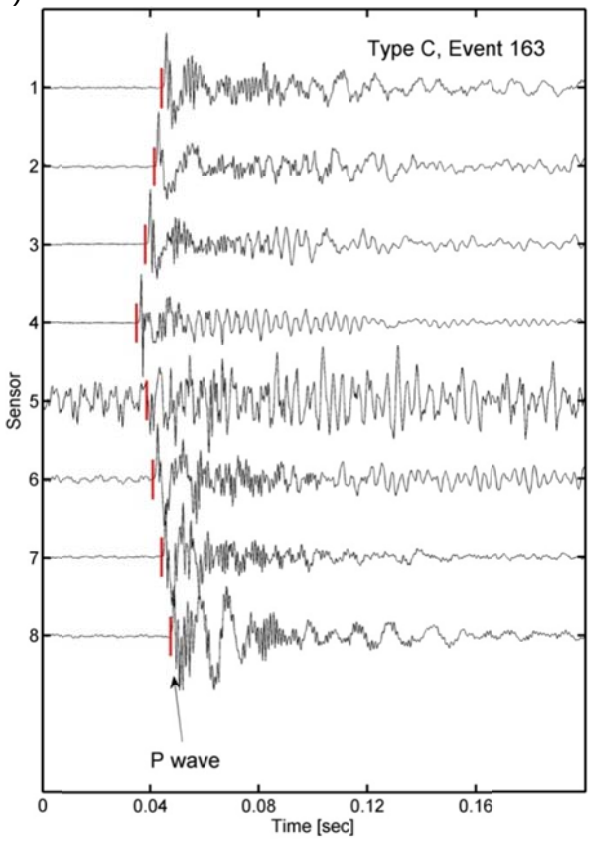
Type C, Event 163
Sensor
1
2
3
4
5
6
7
8
P wave
0
0.04
0.08
0.12
0.16
Time [sec]

g)

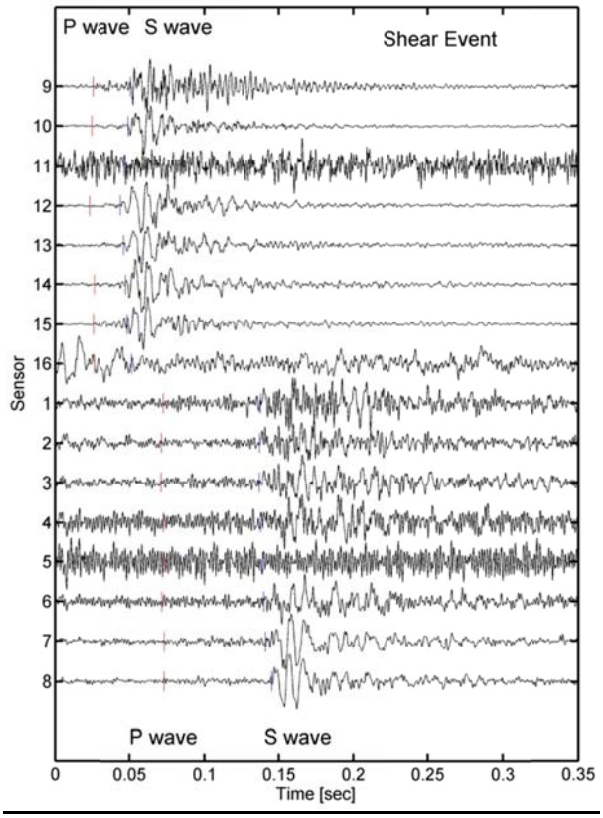
P wave S wave
Shear Event
Sensor
9
10
11
12
13
14
15
16
1
2
3
4
5
6
7
8
P wave
S wave
0
0.05
0.1
0.15
0.2
0.25
0.3
0.35
Time [sec]

Figure 6

a)

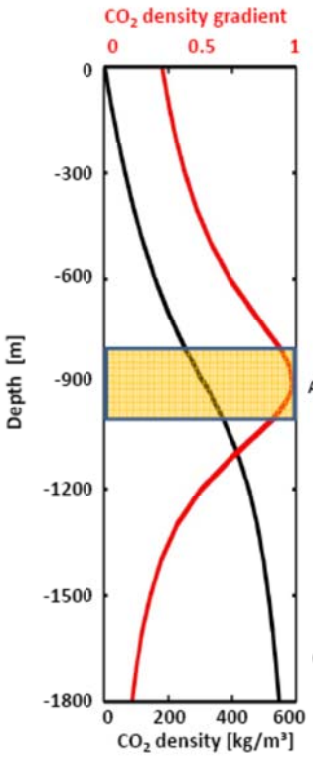
CO_2 density gradient
0
0.5
1
0
-300
-600
-900
-1200
-1500
-1800
Depth [m]
0
200
400
600
CO_2 density [kg/m³]

b)

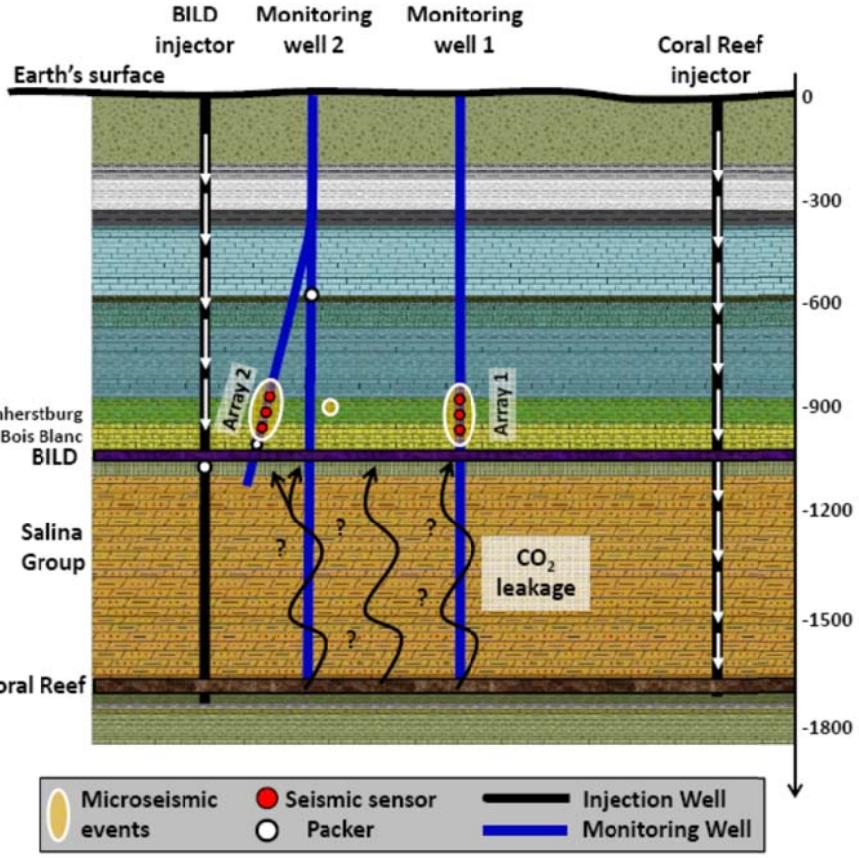
BILD injector
Monitoring well 2
Monitoring well 1
Coral Reef injector
Earth's surface
0
-300
-600
-900
-1200
-1500
-1800
Array 2
Array 1
Amherstburg
Bois Blanc
BILD
Salina Group
Coral Reef
CO_2 leakage
?
Microseismic events
Seismic sensor
Packer
Injection Well
Monitoring Well

Figure 7